Fabrication of Gold-Graphitic Carbon Nitride Composite Electrode for the Detection of Pimobendan

Hsiang-Ning Luk , Xu-Jia Chang , Ren-Jang Wu *

Posted Date: 26 June 2023

doi: 10.20944/preprints202306.1748.v1

Keywords: electrochemical; sensor; Au/g-C3N4; pimobendan

Article

Fabrication of Gold-Graphitic Carbon Nitride Composite Electrode for the Detection of Pimobendan

Hsiang-Ning Luk[1], Xu-Jia Chang[2] and Ren-Jang Wu*[,2]

[1] Department of Anesthesia, Hualien Tzu-Chi Hospital, Hualien 97002, Taiwan

[2] Department of Applied Chemistry, Providence University, Shalu, Taichung 43301, Taiwan

* Correspondence: rjwu@pu.edu.tw; Tel.: +886-4-26328001-15212

Abstract: In this study, the preparation of the composite 3% Au/graphite-C_3N_4 (3% Au/g-C_3N_4) sensing material was prepared by doping 3% Au onto the surface of graphitic carbonitride (C_3N_4) for detection pimobendan. By the way of sensing materials characterization, the X-ray diffraction analysis (XRD), transmission electron microscope (TEM), scanning electron microscope (SEM), energy-dispersive X-ray spectroscopy (EDS) and Fourier-transform infrared spectroscopy (FTIR) were performed. The cyclic voltammetry (CV) was used to measure the concentration and redox properties of pimobendan. It can be seen that when the voltage value is 0.05 V, and a reduction peak was appeared and the pimobendan concentration (0 to 55 μM) has a relationship with the reduction current value. At low concentrations of pimobendan concentration from 0.0 to 0.8 μM, the linearity R^2 = 0.9642 with a detection limit of 0.28 μM. A possible pimobendan sensing mechanism on 3% Au/g-C_3N_4 was proposed.

Keywords: electrochemical; sensor; Au/g-C_3N_4; pimobendan

1. Introduction

Heart failure is an increasing public health problem, mainly in the elderly, and is one of the important sources of death and hospitalization in elderly patients. The cardiotonic drug pimobendan ($C_{19}H_{18}N_4O_2$) in Figure 1(a) is a calcium sensitizer and selective inhibitor of phosphodiesterase III, studies have shown that as a canine cardiotonic therapy can increase lifespan [1]. Pimobendan is a drug licensed for veterinary use indicated for the treatment of heart failure in dogs and it is also used in Japan in human patients [1]. Oral pimobendan is used for treating congestive heart failure (CHF) in dogs and cats [2]. Pimobendan is current in patients with chronic heart failure but is less effective in patients with old myocardial infarction (OMI) than in patients with dilated cardiomyopathy (DCM) or other heart diseases [3,4].

Currently used for clinical analysis of pimobendan is by high performance liquid chromatography (HPLC) [5] and Liquid Chromatography Tandem Mass Spectrometry (LC/MS) [6]. It is time-consuming (more than a few minutes), expensive equipment, and the coexistence of many complex sample preparations that interfere with the actual sample, that is not suitable for tests that require a large number of samples in a short analysis time.

To our knowledge, the fast detections of pimobendan by electrochemical method have not been studied. Therefore, it is hoped to develop a cardiotonic drug measurement with high sensitivity, high selectivity and high long-term stability by cyclic voltammetry and differential pulse voltammetry in electrochemical systems. This study is expected to gain a deeper understanding of the mechanisms of adsorption and surface redox reactions during cardiotonic drug sensing. Electrochemical detection technique has been considered as an outstanding candidate for the determination of pimobendan n owing to its advantages such as excellent sensitivity, high selectivity, fast response, simple operation and cost-effective.

Graphite carbonitride (g-C_3N_4) is a planar two-dimensional sheet structure similar to graphene, which is a typical polymer semiconductor. Due to its special structure and excellent properties, g-C_3N_4 has become a popular material for research of some electrochemical reactions [7-

Preprints (www.preprints.org) | NOT PEER-REVIEWED | Posted: 26 June 2023 doi:10.20944/preprints202306.1748.v1

9]. Since g-C_3N_4 has attracted consideration in various fields due to its excellent optical properties, high thermal stability in basic/acidic media, earth abundance and environmentally friendly nature [10]. However low conductivity of g-C_3N_4 limits its application in electrochemical electrode, to overcome this deficiency to dope the metal is a way to improve its conductivity [11].

Among nanomaterials, gold nanoparticles is functional material that has received increased attention [12]. Gold has been used in promotion of some oxidation reactions and electrochemical reaction system [12]. Until now, the Au-based nanomaterials have been observed as dynamic nanostructured materials and expected to be important element for electrode device [12]. Therefore, the main objective of the present work was to establish a simplified cyclic voltammetry method for determination of pimobendan using electrochemical sensors based on Au/g-C_3N_4/glassy carbon electrode. The morphology, crystal phase, chemical component and microstructure of the as-prepared electrochemical sensors were characterized using various techniques like XRD (X-ray diffraction) and TEM (transmission electron microscopy). Moreover, the electrochemical behavior of the as-synthesized electrochemical sensors was investigated by cyclic voltammetry.

2. Experimental section

2.1. Chemicals and reagent

Melamine (99%), Methyl alcohol (99%) and tetrachloroauric acid trihydrate (99%) were purchased from Alfa Aesar Co., Ltd. Chitosan (>75%), Sodium phosphate dibasic (99%), Potassium phosphate monobasic (99%), Potassium chloride (99%) and Sodium chloride (99%) were obtained from SIGMA ALDRICH Company. The reagents used in the experiment were analytically pure without further purification. The laboratory-grade distilled and deionized water (Millpore, Milli-Q Water Purification System) was used throughout the experiment.

2.2. Electrochemical sensors preparation

A facile method for the fabrication of electrochemical sensors and the construction process is as behind. Take melamine for gradient calcining to obtain g-C_3N_4 of light yellow powder. Then take g-C_3N_4, add appropriate amount of tetrachloroauric acid ($HAuCl_4$) solution and methanol (Methyl alcohol), heat and stir until powdery. Then the powers were dried, and carried out gradient calcination to obtain a light gray powder of various percentages of Au/g-C_3N_4 products. To shake and mix Au/g-C_3N_4 and chitosan solution evenly, and then was coating on the surface of the glassy carbon electrode. After drying to form a film, the preparation of the working electrode was completed.

2.3. Characterization apparatus

The crystal structures of the preparation samples were characterized by X-ray diffraction (XRD) using a Bruker D8 focus diffractometer operating at 35 kV and 35 mA with a scan step of 2°/min between 10° and 80° (2θ), using Cu Kα radiation (Cu Kα1, 1.5404Å). The microstructure and morphology of the samples were performed using JEM-2010 (JEOL, Japan, 200 kV) transmission electron microscope and scanning electron microscope FESEM/ Energy-dispersive X-ray spectroscopy (EDS) (JEOL JSM-7500F, JSM-6500F, Japan, 15 kV). Fourier transform infrared (FTIR) spectroscopy was by using an Agilent Cary 630 ATR-FTIR spectrophotometer (USA).

2.4. Electrode preparation and electrochemical measurements

Prior to use, the surface of the bare electrode (glasses carbon electrode, GCE) was successively polished with aluminum oxide powder on a polishing cloth to a mirror finish and rinsed with water. As shown in Figure 1(b), the electrochemical sensing system includes three electrodes and an electrochemical workstation. Pt and Ag/AgCl were used as the counter and reference electrodes, respectively. G-C_3N_4 and Au/g-C_3N_4 electrodes were used as the working electrode. All electrochemical measurements were performed out on a ZIVE SP1 compact type electrochemical workstation (Won A Tech/ZIVE LAB). The scanning range was from -1.0 to 1.0 V at a rate from 10

Preprints (www.preprints.org) | NOT PEER-REVIEWED | Posted: 26 June 2023 doi:10.20944/preprints202306.1748.v1

to 200 mVs^{-1} by using cyclic voltammetry (CV) method. The detection limit (DL) is measured as DL = (3×SD)/m, where SD is the standard deviation of the blank sample signal and the m is revealed the slope of the response curve versus pimobendan concentration (range from 0.0 to 55 μM).

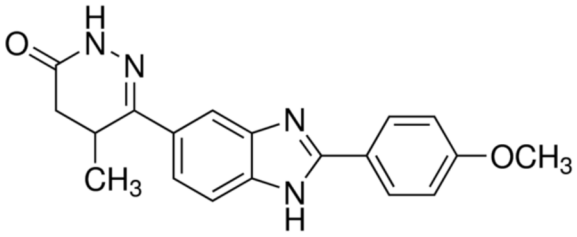

(a)

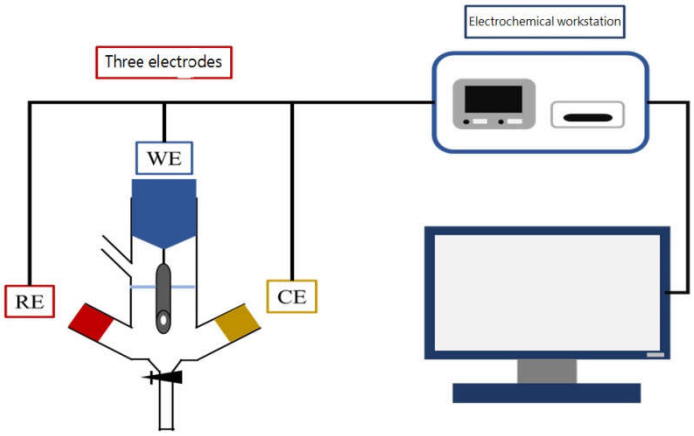

(b)

Figure 1. (a) Chemical structure of pimobendan (b) The electrochemical detection system.

3. Results and Discussion

3.1. Characterized the sensing materials

To investigate the structure of g-C_3N_4 and Au/g-C_3N_4, the XRD patterns of g-C_3N_4 and Au/g-C_3N_4 with different Au contents (1%, 3% and 5%) were studied. As can be seen in Figure 2, g-C_3N_4 XRD has clear peaks (100) and (002) at 2θ = 13.1° and 27.3°, respectively. These represent the accumulation of conjugated π-π bonds in the aromatics of graphite carbonitrides [7]. Furthermore in Figure 2, the characteristic peaks at 37.7°, 44.0°, 64.3°, and 77.4° correspond to the crystalline planes of Au(111), Au(200), Au(220) and Au(311), respectively [8]. From this, it can be seen that the characteristic peak of Au (111) increases with the increase of the proportion of Au doping, so it is known that Au has been successfully doped onto the g-C_3N_4 flakes. By using Scherer's formula, the calculated average crystalline sizes of Au (111) of 3% Au/C_3N_4 was found to be approximately 18.6 nm.

Preprints (www.preprints.org) | NOT PEER-REVIEWED | Posted: 26 June 2023 doi:10.20944/preprints202306.1748.v1

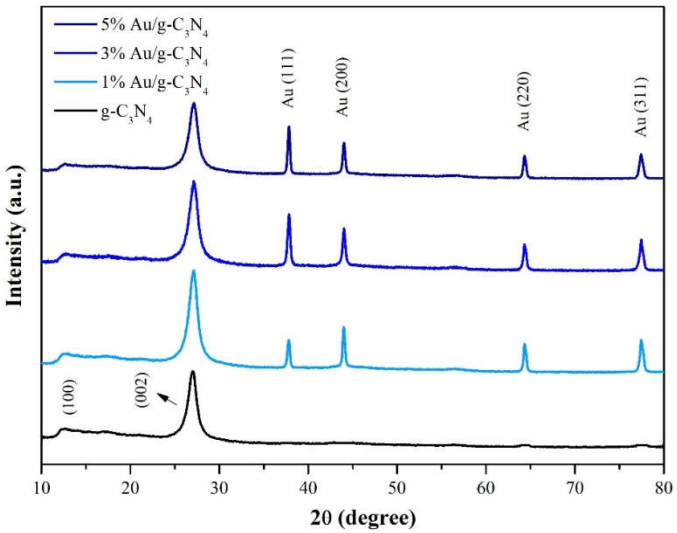

Figure 2. XRD patterns of g-C_3N_4, 1% Au/g-C_3N_4, 3% Au/g-C_3N_4 and 5% Au/g-C_3N_4.

Figure 3(a) presents a g-C_3N_4 TEM with a magnification and scale bar 1000 nm, and (b) shows a g-C_3N_4 TEM with a magnification and the scale bar 500 nm. It can be seen from the figure that g-C_3N_4 presents a multilayer sheet structure. Figure 4(a) is a g-C_3N_4 TEM with a magnification and scale bar 500 nm, and (b) is a g-C_3N_4 TEM with a magnification and scale bar 10 nm. We can see from Figure 4(b) where Au is doped on the surface of flake g-C_3N_4. The lattice line is used to calculate the lattice spacing of Au and compared with the literature. It is found that the Au (111) crystal plane has a lattice spacing of d = 0.225 nm [9]. It can be seen that the spherical Au is successfully doped on the flake g-C_3N_4, the average crystalline size of Au (111) is calculated as 19.2 nm. It reveals similar result of XRD spectra in Figure 2.

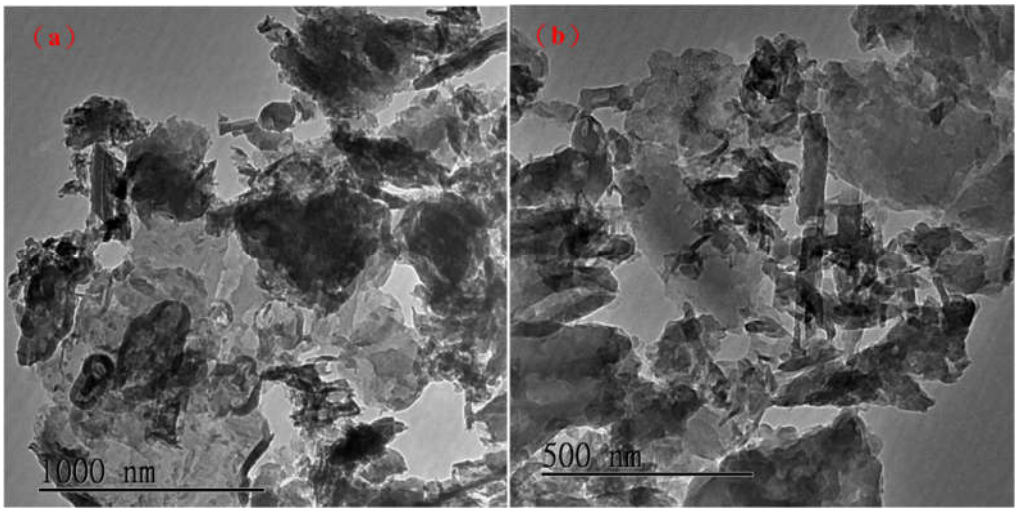

Figure 3. TEM images of (a) g-C_3N_4 scale bar 1000 nm（b）g-C_3N_4 scale bar 500 nm.

Preprints (www.preprints.org) | NOT PEER-REVIEWED | Posted: 26 June 2023 doi:10.20944/preprints202306.1748.v1

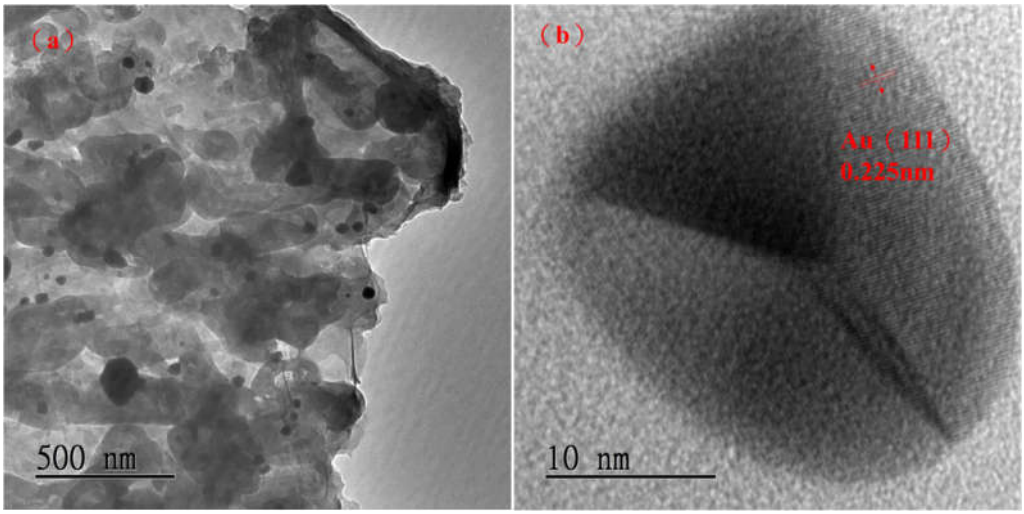

Figure 4. TEM images of (a) 3% Au/g-C_3N_4 scale bar 500 nm (b) 3% Au/g-C_3N_4 scale bar 10 nm.

The microstructure and distribution of elements on samples can be characterized by SEM and EDS instruments. Figure 5a showed a g-C_3N_4 SEM image with a scale bar of 50 μm, and 5b is the g-C_3N_4 SEM image of a scale bar of 20 μm. The surface of g-C_3N_4 exhibited an aggregation from unregular like smaller particles structure in Figure 5a and b. To study the element distribution and composition of as-prepared samples, energy-dispersive X-ray spectroscopy (EDS) was employed. It is revealed a g-C_3N_4 EDS and element mapping images in Figure 6. Figure 6 presents the carbon and nitrogen elements are coexisted in the g-C_3N_4, and the two elements are homogeneously distributed on the surface of the g-C_3N_4. Figure 7a is a 3% Au/g-C_3N_4 SEM image with a scale bar of 50 μm, and 7b is a 3% Au/g-C_3N_4 SEM image with scale bar 20 μm. The 3% Au/g-C_3N_4 showed an aggregation structure from smaller particles in Figure 7a and 7b. Figure 8 shows 3% Au/g-C_3N_4 EDS and mapping images. Figure 8 reveals the carbon, nitrogen and gold elements are coexisted on the 3% Au/g-C_3N_4, and the three elements are homogeneously distributed on the surface of the 3% Au/g-C_3N_4.

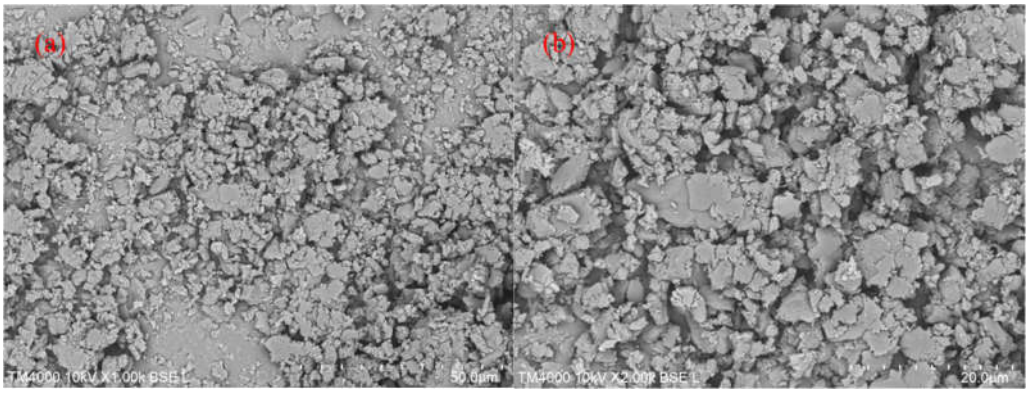

Figure 5. SEM images of (a) g-C_3N_4 scale bar 50 μm (b) g-C_3N_4 scale bar 20 μm.

Preprints (www.preprints.org) | NOT PEER-REVIEWED | Posted: 26 June 2023 doi:10.20944/preprints202306.1748.v1

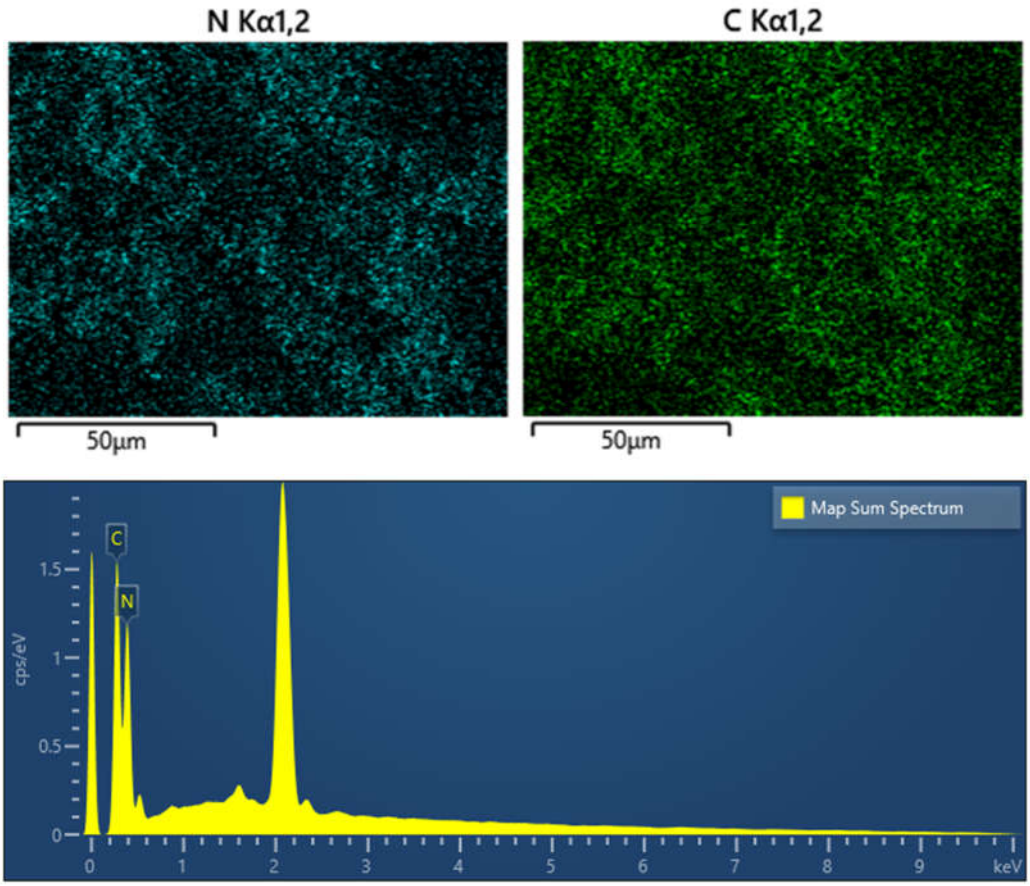

Figure 6. EDS and elements mapping images of g-C_3N_4.

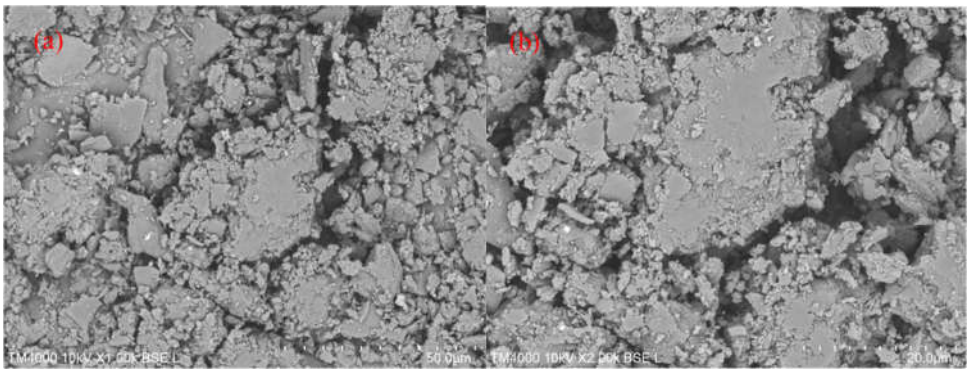

Figure 7. SEM images of (a) 3% Au/g-C_3N_4 scale bar 50 µm (b) 3% Au/g-C_3N_4 scale bar 20 µm.

Preprints (www.preprints.org) | NOT PEER-REVIEWED | Posted: 26 June 2023 doi:10.20944/preprints202306.1748.v1

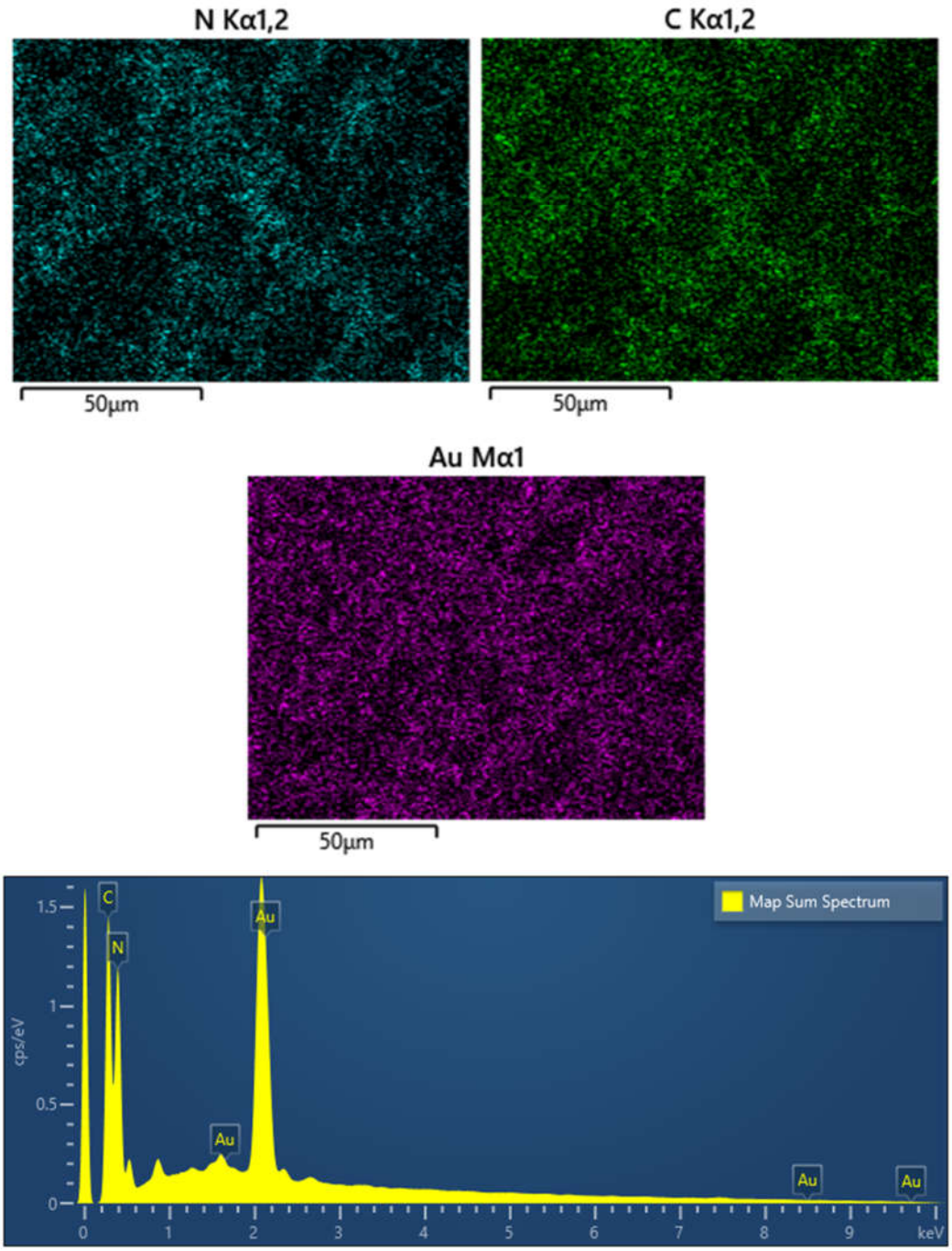

Figure 8. EDS and elements mapping images of 3% Au/g-C_3N_4.

Figure 9 revealed the FTIR spectra of g-C_3N_4, 1% Au/g-C_3N_4, 3% Au/g-C_3N_4 and 5% Au/g-C_3N_4. Where the broadened peaks between 3000 and 3500 cm^{-1} (highest at 3092 cm^{-1}) were correlated to the stretching vibration [13] of remaining free N-H in the bridging C-NH-C units and O-H initiated from physically adsorbed water species on g-C_3N_4 surface, respectively. As shown, the main characteristic group peaks observed in the region from 900 to 1700 cm−1 were usually assigned to stretching vibration signals of aromatic heptazine-derived repeating units, including the typical sp^2 C=N stretching modes at 1627 cm^{-1} and out-of-plane bending vibrations of the sp^3 C-N bonds at 1536, 1393, 1311 and 1229 cm^{-1}[14]. The sharp absorption peak located at about 800 cm^{-1} was attributed to the characteristic ring mode of tri-s-triazine cycles [15], and the absorption band at 881 cm^{-1} was assigned as the deformation mode of N-H in amino groups [13-15], respectively. In Figure 9, no obvious peak was observed by addition of gold on g-C_3N_4.

Preprints (www.preprints.org) | NOT PEER-REVIEWED | Posted: 26 June 2023 doi:10.20944/preprints202306.1748.v1

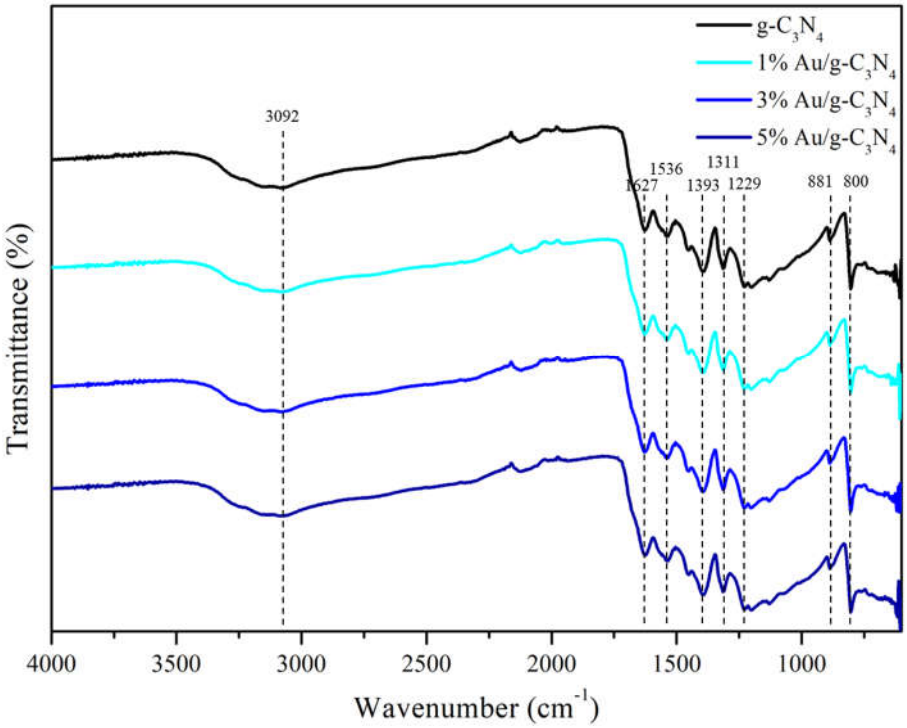

Figure 9. FTIR spectra of g-C_3N_4, 1% Au/g-C_3N_4, 3% Au/g-C_3N_4 and 5% Au/g-C_3N_4.

3.2. Sensing properties

3.2.1. Scan rate effect

To conclude whether the redox process is controlled by a diffusion or adsorption, this study considered the relationship between oxidation current and scan rate. If it appears a linear relationship of peak current with sweep rate, then it usually means an adsorbed pimobendan molecule is controlled [16]. At pH =7.0 the CV method was used of scan rates ranging from 10 to 200 mVs^{-1} on oxidation current intensity at a pimobendan concentration at 55 μM. In Figure 10A, the oxidative current peaks were located at around -0.40 V and 0.40 V and reduction current was found near 0.05 V of 3 %Au/g–C_3N_4 increased with the various scan rates. To determine the relationship between pimobendan current and scan rate, plots of the scan rate versus current intensity in Figure 10B. The scan rate was presented a linear relationship with the anodic peak current (Ipa) at 0.4 V and cathodic peak current (Ipc) at 0.05 V, and it showed the R^2 were obtained as 0.9965 and 0.9968, respectively. In Figure 10C the square root of scan rate exhibited a linear relationship with the anodic peak current (Ipa) and cathodic peak current (Ipc), it presented R^2 = 0.9823 and 0.9822, respectively. Above results showed the redox reaction of pimobendan on the modified electrode was an adsorption-controlled process, indicating that pimobendan was directly adsorption on the electrode surface [16]. We choose the condition of scan rate at 50 mVs^{-1} for it is easily for the peaks separations in Figure 10A.

Preprints (www.preprints.org) | NOT PEER-REVIEWED | Posted: 26 June 2023 doi:10.20944/preprints202306.1748.v1

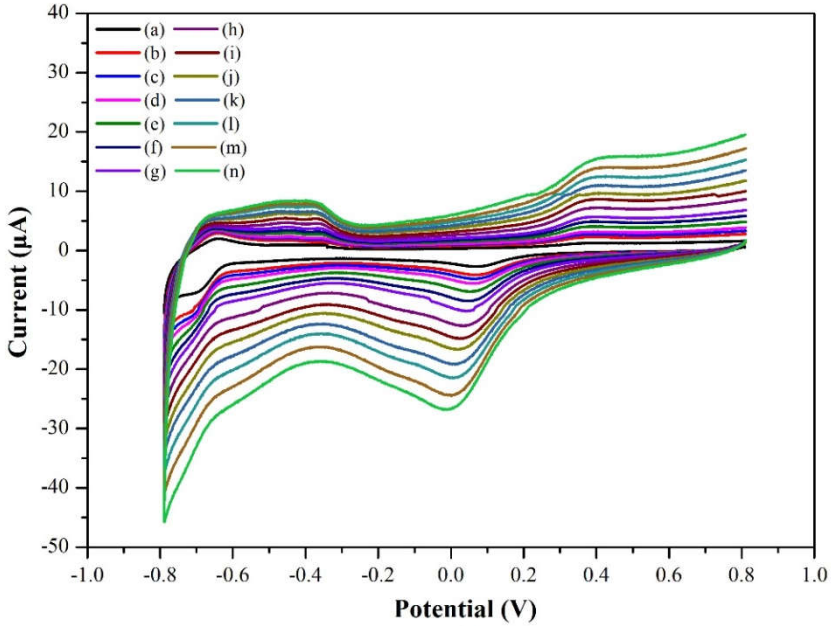

A.

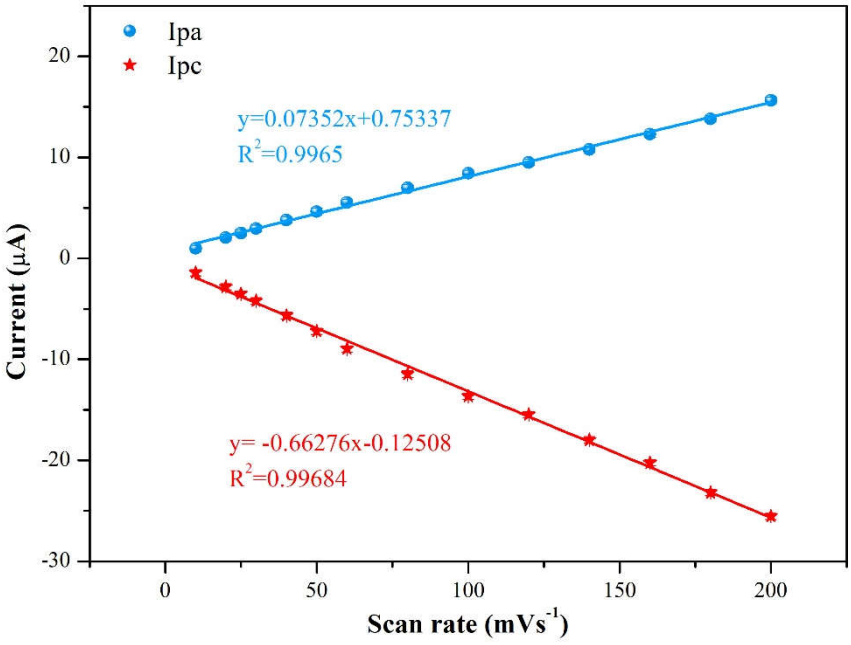

B.

Preprints (www.preprints.org) | NOT PEER-REVIEWED | Posted: 26 June 2023 doi:10.20944/preprints202306.1748.v1

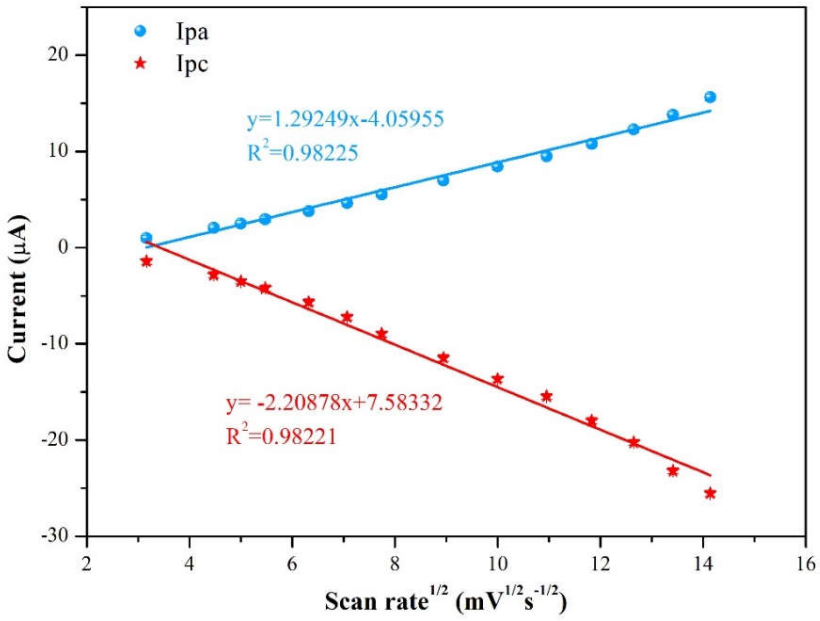

C.

Figure 10. A. Scan rate of 3%Au/g-C_3N_4 at (a) 10 (b) 20 (c) 25 (d) 30 (e) 40 (f) 50 (g) 60 (h) 80 (i) 100 (j) 120 (k) 140 (l) 160 (m) 180 (n) 200 mVs-1, B. The scan rate was presented a linear relationship with the Ipa at 0.4 V and Ipc at 0.05 V, C. The square root of scan rate exhibited a linear relationship with the Ipa at 0.4 V and Ipc at 0.05 V.

3.2.2. Various kind materials of sensing properties

Figure 11A presents CV plots which indicating the current signals of the GCE, g-C_3N_4 electrode and 3%Au/g–C_3N_4 electrode at a scan rate of 50 mV/s and pimobendan concentration of 55 μM at pH=7.0. No significant CV current signal was observed on the GCE, a reduction peak was observed at 0.0 V on g–C_3N_4 electrode in Figure 11A. The 3%Au/g-C_3N_4 composite had the highest oxidation peak current at approximately 0.4 V and reduction peak at 0.05 V.

In Figure 11B, the oxidation peaks were placed at around -0.40 V and 0.40 V which were identified as the oxidative products from pimobendan in Figure 11B (a) and (b) [17]. And reduction peak was found at 0.10 V which was identified as the pimobendan from the oxidative products [17].

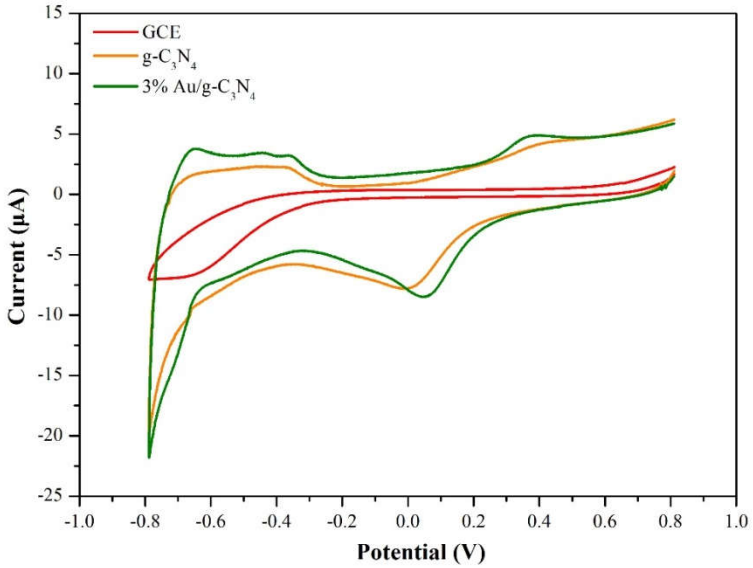

A.

Preprints (www.preprints.org) | NOT PEER-REVIEWED | Posted: 26 June 2023 doi:10.20944/preprints202306.1748.v1

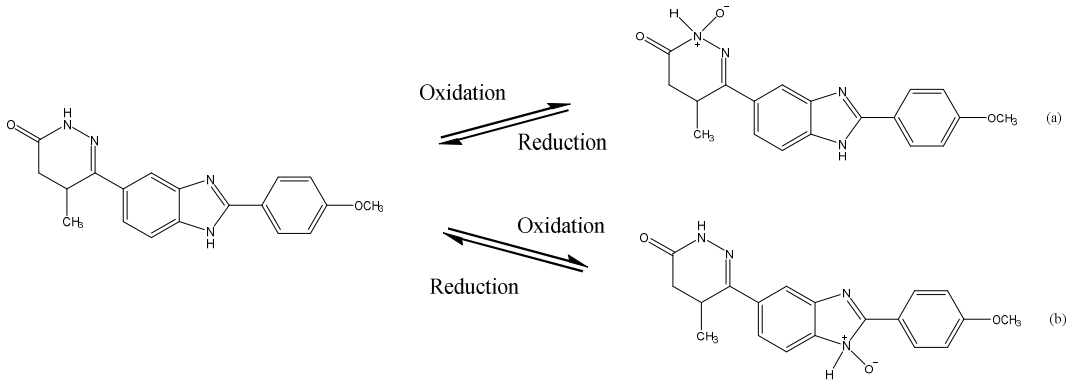

B.

Figure 11. A CV plots of the GCE, g-C_3N_4 electrode and 3 %Au/g–C_3N_4 electrode at a scan rate of 50 mV/s and pimobendan concentration of 55 μM at pH=7.0. B. The possible oxidation and reduction reactions of pimobendan.

3.2.3. CV current versus concentration

Figure 12A revealed the CV currents versus pimobendan concentrations (ranging from 0.0 to 55 μM). It showed the 3 %Au/g-C_3N_4 at higher concentrations (Figure 12A) the reduction peak current (cathodic peak current) exhibited a higher current value. From low concentration of pimobendan (0.0–0.84 μM) indicating a linear relationship between the cathodic peak current and the pimobendan concentrations in Fig. 12B. It was obtained the R^2 as 0.9642, and the detection limit was calculated to 0.28 μM.

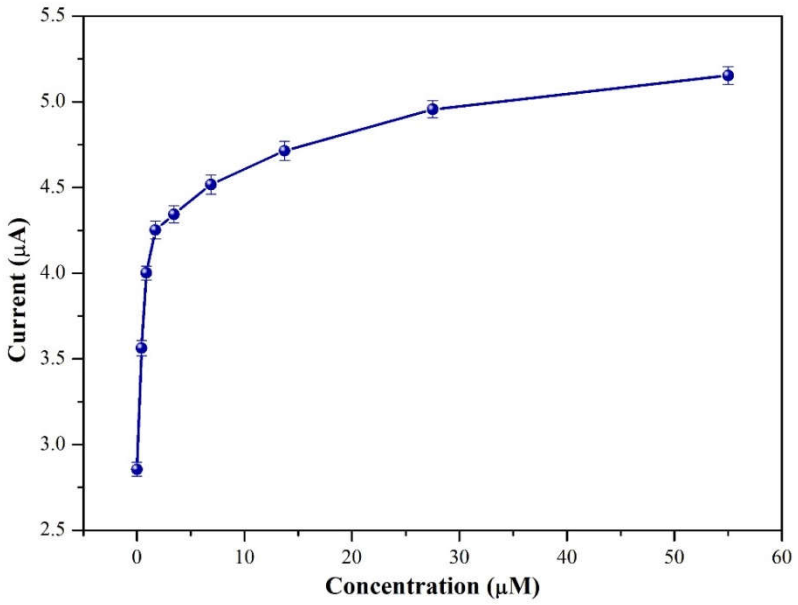

A.

Preprints (www.preprints.org) | NOT PEER-REVIEWED | Posted: 26 June 2023 doi:10.20944/preprints202306.1748.v1

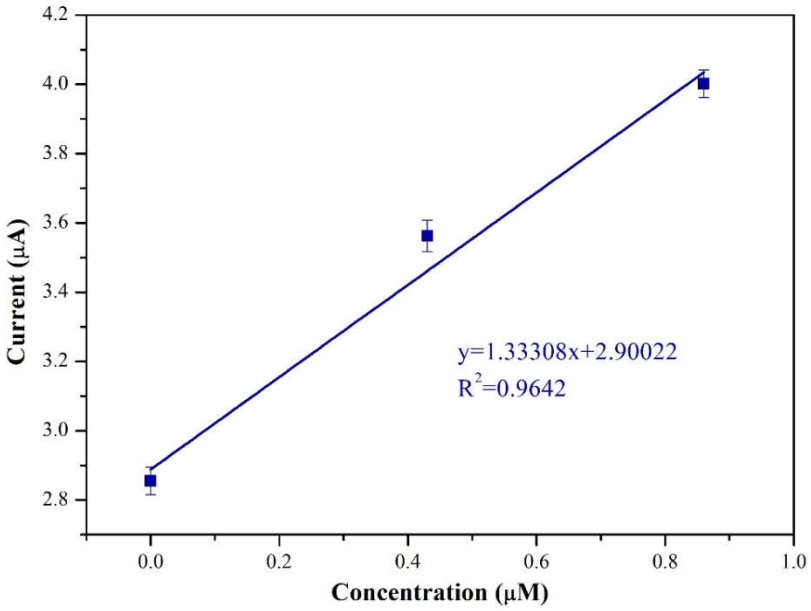

B.

Figure 12. A. CV currents versus pimobendan concentrations ranging from 0.0 to 55 μM on 3%Au/g-C_3N_4 at a scan rate of 50 mV/s and pH=7.0, B. A linear relationship between the cathodic peak current and the pimobendan concentrations.

3.2.4. Interference effect

From the literature, the interferences of 55 μM dopamine (DA), 55 μM epinephrine (EP) and 55 μM uric acid (UA) are naturally coexist in physiological samples. Accordingly, the interference tests by plotting the CV reduction current versus some interferences materials of DA, EP and UA was displayed in Figure 13. The CV current of pimobendan (4.7 μA) was higher than those of DA (0.38 μA), EP (0.51 μA) and UA (0.49 μA) at the same concentration in Figure 13. It presented the sensing material of pimobendan detection was high selectivity and little interferences with DA, EP and UA.

Preprints (www.preprints.org) | NOT PEER-REVIEWED | Posted: 26 June 2023 doi:10.20944/preprints202306.1748.v1

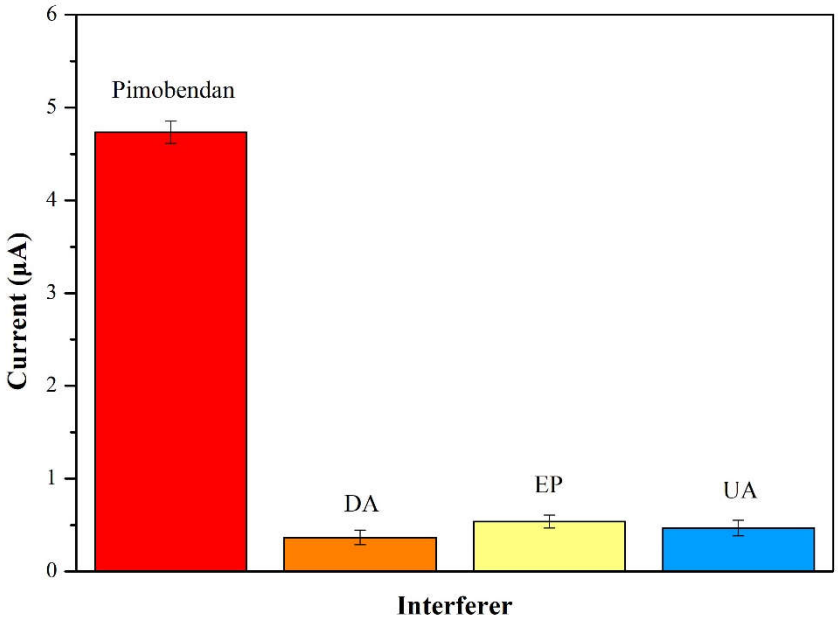

Figure 13. The interference effect for 55 μM pimobendan of 55 μM dopamine (DA), 55 μM epinephrine (EP) and 55 μM uric acid (UA) at a scan rate of 50 mV/s and pH=7.0.

3.3. Sensing mechanism

The 3 %Au/g-C_3N_4 composite had the highest oxidation peak current at approximately 0.4 V and reduction peak at 0.05 V in Figure 11A. The redox reaction mechanisms of the pimobendan sensing under the amide oxidation and amide oxide reduction reactions on the Au/g-C_3N_4 electrode are illustrated in Figure 14 [17-21]. The C_3N_4 showed a flake-like morphology of TEM images in Figure 3 and Figure 4. Graphitic carbon nitride (g-C_3N_4) is a two-dimensional organic semiconductor with a high specific surface area, additionally g-C_3N_4 owns high electrical conductivity for its sole delocalized conjugated structure [22-26]. Au is applied in promotion of some oxidation-reduction reactions and electrochemical reaction system [12,16,21]. The binding of pimobendan molecules on nano Au increased the electron transfer, yielding the modification in response current. The presence of Au, therefore, enhanced the detection of oxidation and reduction current sensitivity [26-30]. The high sensing circuit of the electrode was feasibly (Figure 11) because the Au nanoparticles on the surfaces of C_3N_4 efficiently collected the pimobendan oxidation–induced electrons during the electrocatalytic reaction and transferred them to the C_3N_4 composite and then to the surface of the GCE [18]. Two possible products of pimobendan (amide) oxidation on the Au catalyst are presented in Figure 14 [17,19,20].

Preprints (www.preprints.org) | NOT PEER-REVIEWED | Posted: 26 June 2023 doi:10.20944/preprints202306.1748.v1

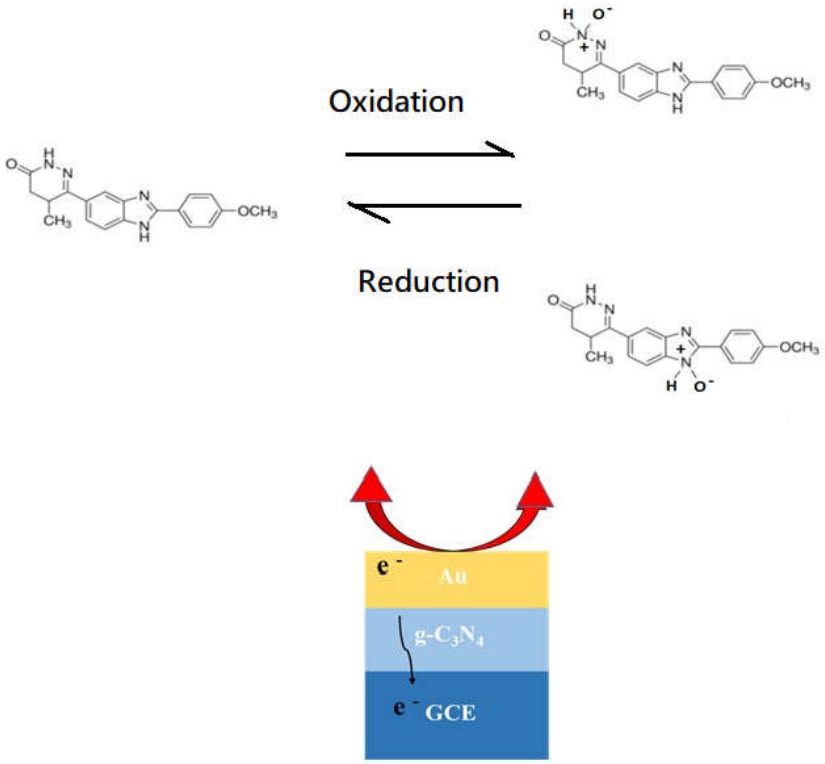

Figure 14. Sensing mechanism of pimobendan on Au/g-C_3N_4 modified electrode.

4. Conclusions

The composite 3% Au/g-C_3N_4 sensing electrode was fabricated for detection pimobendan. The Sensing materials characterization by XRD and TEM. The cyclic voltammetry was applied to detect the concentration and redox properties of pimobendan. It can be seen that when the voltage value is 0.05 V, and a reduction peak was presented and the pimobendan concentration from 0 to 55 μM has a relationship with the reductive currents. At low concentrations of pimobendan concentration from 0.0 to 0.8 μM, the linearity $R^2 = 0.9642$ with a detection limit of 0.28 μM. Little interferences of DA, EP and UA were detected with pimobendan. A possible pimobendan sensing mechanism on 3% Au/g-C_3N_4 was proposed.

Author Contributions: Conceptualization, H.-N.L. and R.-J.W.; methodology, R.-J.W.; software, X.-J.C.; validation, X.-J.C.; formal analysis, X.-J.C.and H.-J.Z; investigation, R.-J.W.; data curation, X.-J.C.; writing—original draft preparation, R.-J.W.; writing—review and editing, H-N.L. and R.-J.W.; supervision, R.-J.W.; project administration, R.-J.W.; funding acquisition, R.-J.W. All authors have read and agreed to the published version of the manuscript. All authors have read and agreed to the published version of the manuscript.

Funding: This research was funded by the National Science and Technology council (Grant No.: NSTC 111-2113-M-126-003), Taiwan, R.O.C, for funding this study.

Data Availability Statement: The data presented in this study are available on request from the corresponding author.

Acknowledgments: The authors are thankful to the National Science and Technology council (Grant No.: NSTC 111-2113-M-126-003), Taiwan, R.O.C, for funding this study. We are also thankful Prof. Hong-jian Zhao

for her kind help for this research work.

Conflicts of Interest: The authors declare no conflict of interest.

Abbreviations

The following abbreviations are used in this manuscript:

XRD X-ray diffraction analysis
TEM Transmission electron Microscope
CV cyclic voltammetry

References

1. Mathieu Magnin, Jeanne Marie Bonnet-Garin, Chiara Laurenza, Caroline Didier, Morgane Gavet, Alexandra Nectoux, Bernard Allaouchiche, St´ephane Junot, Evaluation of pimobendan effect on sublingual microcirculation in an experimental pharmacology induced hypotension porcine model, Research in Veterinary Science 148 (2022) 7–14. https://doi.org/10.1016/j.rvsc.2022.03.021
2. L.V. Kost, T.M. Glaus, A. Diana, M. Baron Toaldo, Effect of a single dose of pimobendan on right ventricular and right atrial function in 11 healthy cats, Journal of Veterinary Cardiology 37 (2021) 52-61. DOI: 10.1016/j.jvc.2021.08.006
3. N. Takeda, Y Hayashi, T Arino, A Takeda, K Noma, Effect of pimobendan in patients with chronic heart failure, Exp Clin Cardiol. 2001 Winter; 6(4): 195–199. PMCID: PMC2858999
4. Hiroaki Kawano, Shuji Arakawa, Osami Satoh, Yuji Matsumoto, Motonobu Hayano, Daisuke Nakatomi, Toshihiko Yamasa, Koji Maemura, Effect of pimobendan in addition to standard therapy for heart failure on prevention of readmission in elderly patients with severe chronic heart failure, Geriatr Gerontol Int 2014;14:109–114. DOI: 10.1111/ggi.12067
5. Jiwoong Her, Kendon W. Kuo, Randolph L. Winter, Crisanta Cruz-Espindola, Lenore M. Bacek, Dawn M. Boothe, Pharmacokinetics of Pimobendan and Its Metabolite O-Desmethyl-Pimobendan Following Rectal Administration to Healthy Dogs, Front Vet Sci. 7 (2020) 423. DOI: 10.3389/fvets.2020.00423
6. Nakkawee Saengklub, Tussapon Boonyarattanasoonthorn, Anusak Kijtawornrat, Doungdaw Chantasart, Preliminary Bioequivalence of an Oral Pimobendan Solution Formulation with Reference Solution Formulation in Beagle Dogs, Vet. Sci. 2022, 9, 141. https://doi.org/10.3390/vetsci9030141
7. Jitong Yan, Yanyan Liu, Runan Wang, Meirong Xia, Jing Wang, Faming Gao, Yongfu Tang, Bamboo-like carbonitride nanotubes with multi-type active sites for oxygen reduction reaction in both alkaline and acid mediums, International Journal of Hydrogen Energy 47 (2022) 7949-7960. https://doi.org/10.1016/j.ijhydene.2021.12.118
8. Dongyan Tian, Jie Wang, Qiandong Zhuang, Songmei Wu, Yu Yu, Kejian Ding, An electrochemiluminescence biosensor based on Graphitic carbon nitride luminescence quenching for detection of AFB1, Food Chemistry 404 (2023) 134183. https://doi.org/10.1016/j.foodchem.2022.134183
9. Fangmu Qua, Magdalena Graczyk-Zajac, Dragoljub Vrankovic, Nan Chai, Zhaoju Yu, Ralf Riedel, Effect of morphology of C-rich silicon carbonitride ceramic on electrochemical properties of sulfur cathode for Li-S battery, Electrochimica Acta 384 (2021) 138265. https://doi.org/10.1016/j.electacta.2021.138265
10. Javad Safaei, Nurul Aida Mohamed, Mohamad Firdaus Mohamad Noh, Mohd Fairuz Soh, Norasikin Ahmad Ludin, Mohd Adib Ibrahim, Wan Nor Roslam Wan Isahak, Mohd Asri Mat Teridi, Graphitic carbon nitride (g-C_3N_4) electrodes for energy conversion and storage: a review on photoelectrochemical water splitting, solar cells and supercapacitors, J. Mater. Chem. A, 2018,6, 22346-22380. https://doi.org/10.1039/C8TA08001A
11. Haoye Wang, Aijuan Xie, Shuji Li, Jiajun Wang, Kaixuan Chen, Zilong Su, Ningning Song, Shiping Luo, Three-dimensional g-C_3N_4/MWNTs/GO hybrid electrode as electrochemical sensor for simultaneous determination of ascorbic acid, dopamine and uric acid, Analytica Chimica Acta 1211 (2022) 339907. https://doi.org/10.1016/j.aca.2022.339907

12. Samarjeet Siwal, Nishu Devi, Venkata K. Perla, Sarit K. Ghosh, Kaushik Mallick, Promotional role of gold in electrochemical methanol oxidation, Catalysis, Structure & Reactivity 5 (2019) 1-9. https://doi.org/10.1080/2055074X.2019.1595872
13. Wee-Jun Ong, Lling-Lling Tan, Yun Hau Ng, Siek-Ting Yong, Siang-Piao Chai, Graphitic Carbon Nitride (g-C3N4)-Based Photocatalysts for Artificial Photosynthesis and Environmental Remediation: Are We a Step Closer To Achieving Sustainability, Chem Rev. 116 (2016) 7159–7329. https://pubs.acs.org/doi/10.1021/acs.chemrev.6b00075
14. Federica Fina, Samantha K. Callear, George M. Carins, John T. S. Irvine, Structural Investigation of Graphitic Carbon Nitride via XRD and Neutron Diffraction, Chem. Mater. 27 (2015) 2612–2618. https://pubs.acs.org/doi/10.1021/acs.chemmater.5b00411
15. PanelJiuqing Wen, Jun Xie, Xiaobo Chen, Xin Li, A review on g-C_3N_4-based photocatalysts, Applied Surface Science 391 (2017) 72-123. https://doi.org/10.1016/j.apsusc.2016.07.030
16. Zhen Zhu, Hsiang-Ning Luk, Yu-Shih Liu, Ren-Jang Wu, Ming-Hung Chung, Xu-Jia Chang, Preparation of Bimetallic Au-Pd/MWCNTs Electrode for Detection of Dopamine, Minerals 12 (2022) 1145. https://doi.org/10.3390/min12091145
17. Zhen Zhu, Hsiang-Ning Luk, Yi-Min Huang, Yu-Cheng Zhang, Xu-Jia Chang, Ren-Jang Wu, Silver/graphene–polypyrrole composite for levosimendan detection, Journal of Chinese Chemical Society 70 (2023) 928-937. https://doi.org/10.1002/jccs.202300001
18. Ye-Cheng Li, Xiao-Song Li, Bin Zhu, Ai-Min Zhu, Boosting low-temperature water gas shift reaction over Au/TiO_2 nanocatalyst activated by oxygen plasma, Chemical Engineering Journal 430 (2021) 133013. https://doi.org/10.1016/j.cej.2021.133013
19. R. Garg, S. Mondal, L. Sahoo, C. P. Vinod, U. K. Gautam, Nanocrystalline Ag_3PO_4 for Sunlight- and Ambient Air-Driven Oxidation of Amines: High Photocatalytic Efficiency and a Facile Catalyst Regeneration Strategy, ACS Appl. Mater. Interfaces 12 (2020) 29324. https://doi.org/10.1021/acsami.0c05961
20. D. Bernier, U. K. Wefelscheid, S. Woodward, Organic Preparations and Procedures International 41 (2009) 175. https://doi.org/10.1080/00304940902955756
21. Ting Xiao, Jianshe Huang, Dewen Wang, Tian Meng, Xiurong Yang, Au and Au-Based nanomaterials: Synthesis and recent progress in electrochemical sensor applications, Talanta 206 (2020) 120210. https://doi.org/10.1016/j.talanta.2019.120210
22. Atefeh Nasri, Babak Jaleh, Milad Daneshnazar, Rajender S. Varma, Sensing Properties of g-C_3N_4/Au Nanocomposite for Organic Vapor Detection, Biosensors 13 (2023) 315. https://doi.org/10.3390/bios13030315
23. Furong Chen, Layue Bao, Ying Zhang, Ruili Wang, Jinghai Liu, Wenfeng Hai, Yushuang Liu, NiCoP/g-C_3N_4 Nanocomposites-Based Electrochemical Immunosensor for Sensitive Detection of Procalcitonin, Sensors 23 (2023), 4348. https://doi.org/10.3390/s23094348
24. Mehrab Pourmadadi, Maryam Rajabzadeh-Khosroshahi, Fatemeh Saeidi Tabar, Narges Ajalli, Amirmasoud Samadi, Mahsa Yazdani, Fatemeh Yazdian, Abbas Rahdar, Ana M. Díez-Pascual, Two-Dimensional Graphitic Carbon Nitride (g-C_3N_4) Nanosheets and Their Derivatives for Diagnosis and Detection Applications, J. Funct. Biomater. 13 (2022) 204. https://doi.org/10.3390/jfb13040204
25. Shaolin Zhang, Nguyen Thuy Hang, Zhijun Zhang, Hongyan Yue, Woochul Yang, Preparation of g-C_3N_4/Graphene Composite for Detecting NO_2 at Room Temperature, Nanomaterials 7 (2017) 12. https://doi.org/10.3390/nano7010012
26. Sanjida Yeasmin, Bo Wu, Ye Liu, Ahasan Ullah, Li-Jing Cheng, Nano gold-doped molecularly imprinted electrochemical sensor for rapid and ultrasensitive cortisol detection, Biosensors and Bioelectronics 206 (2022) 114142. https://doi.org/10.1016/j.bios.2022.114142
27. Saied Jafari, Mohammad Dehghani, Navid Nasirizadeh, Mostafa Azimzadeh, An azithromycin electrochemical sensor based on an aniline MIP film electropolymerized on a gold nano urchins/graphene oxide modified glassy carbon electrode, Journal of Electroanalytical Chemistry 829 (2018) 27-34. https://doi.org/10.1016/j.jelechem.2018.09.053
28. Mari Elancheziyan, Sellappan Senthilkumar, Redox-active gold nanoparticle-encapsulated poly(amidoamine) dendrimer for electrochemical sensing of 4-aminophenol, Journal of Molecular Liquids 325 (2021) 115131. https://doi.org/10.1016/j.molliq.2020.115131
29. Yongying Zhou, Jin Zhao, Shenghua Li, Minjie Guo, Zhi Fan, An electrochemical sensor for the detection of p-nitrophenol based on a cyclodextrin-decorated gold nanoparticle–mesoporous carbon hybrid, Analyst 144 (2019) 4400-4406. DOI: 10.1039/C9AN00722A

 doi:10.20944/preprints202306.1748.v1

30. Jinmei Luo, Shuhuai Li, Yuwei Wu, Chaohai Pang, Xionghui Ma, Mingyue Wang, Chenghui Zhang, Xu Zhi, Bei Li, Electrochemical sensor for imidacloprid detection based on graphene oxide/gold nano/β-cyclodextrin multiple amplification strategy, Microchemical Journal 183 (2022) 107979. https://doi.org/10.1016/j.microc.2022.107979